NANO LETTERS

LETTER

pubs.acs.org/NanoLett

Imaging the Hidden Modes of Ultrathin Plasmonic Strip Antennas by Cathodoluminescence

Edward S. Barnard,[†] Toon Coenen,[‡] Ernst Jan R. Vesseur,[‡] Albert Polman,[‡] and Mark L. Brongersma*[,†]

[†]Geballe Laboratory for Advanced Materials, Stanford University, Stanford, California 94305, United States

[‡]Center for Nanophotonics, FOM Institute AMOLF, Science Park 104, 1098 XG Amsterdam, The Netherlands

ABSTRACT: We perform spectrally resolved cathodoluminescence (CL) imaging nanoscopy using a 30 keV electron beam to identify the resonant modes of an ultrathin (20 nm), laterally tapered plasmonic Ag nanostrip antenna. We resolve with deep-subwavelength resolution four antenna resonances (resonance orders $m = 2-5$) that are ascribed to surface plasmon polariton standing waves that are confined on the strip. We map the local density of states on the strip surface and show that it has contributions from symmetric and antisymmetric surface plasmon polariton modes, each with a very different mode index. This work illustrates the power of CL experiments that can visualize hidden modes that for symmetry reasons have been elusive in optical light scattering experiments.

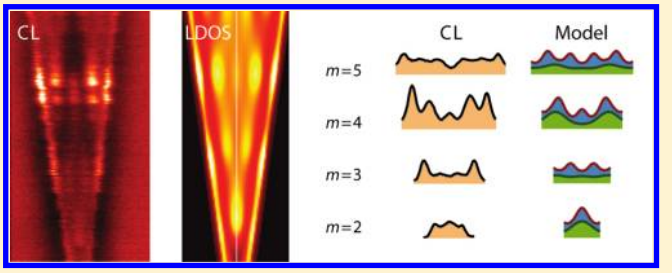

KEYWORDS: Surface plasmon polariton, cathodoluminescence, antenna, LDOS, quantum emitter

Plasmonic antennas are extensively used to control the emission properties of molecules, quantum dots, and other nanoscale emitters[1] by modifying the local density of optical states (LDOS) surrounding the emitter. With nanoscale control of the antenna's size, shape, and dielectric environment, the spectrum, emission rate, polarization, and angular emission profile of optical emitters can be tailored to a great extent. Maps of the LDOS near antennas can provide valuable insights into their operation by linking their geometrical and radiation properties. In this paper, we demonstrate this point for a metal strip antenna whose resonant behavior is governed by surface plasmon polaritons (SPPs) that can propagate back and forth between the two edges of the strip.[2−4] These antennas have previously been shown to resonantly scatter light[5] and effectively enhance absorption in a Si photodetector.[6]

The most common way to study the resonant behavior of antennas is with light scattering experiments. Another possibility is to operate the antenna in a receiving mode, in which case it is used to convert incident free space photons into intense local near-fields. In such experiments, the illumination conditions in terms of the incident beam direction and polarization are very important. For example, symmetry dictates that only a limited set of antenna modes can optically be excited using a normally incident plane wave with its electric field polarized normal to the length of the strip. One way to reveal the other "hidden" modes is by changing the angle of illumination. We will follow another approach, which is to excite the antenna modes with an electron beam and to collect the emission from the structure in all directions. It is important to realize these hidden modes are distinct from dark modes that exhibit a very limited coupling to free space radiation and are invisible in these measurements.[7,8] Dark (nonradiative) modes can be indirectly measured using techniques such as electron-energy loss spectroscopy (EELS) that measure the energy loss spectrum of the incident beam.[9,10]

It is well-known that very thin metal strips such as used here support two distinct types of plasmonic modes that result from coupling between SPPs propagating on the top and bottom surfaces of the strip. One of the coupled modes is a long-range (LR) SPP mode with a symmetric transverse field distribution that exhibits a relatively long propagation length because of its relatively low field overlap with the metal.[11−14] Its counterpart is the antisymmetric, short-range (SR) SPP mode. Both the long- and short-range SPPs can form resonant standing waves across the width of the antenna, and the antenna's radiation properties are thus determined by a combination of these modes. To control and optimize the ultrathin strip antenna characteristics, and to use the antenna in the transmitting mode, detailed knowledge of the excitation of the two SPP modes and their effect on the antennas radiation efficiency is essential.

In this work, we use electron beam excitation to investigate the strip antenna resonances. As we have shown before, electron beam irradiation leads to the excitation of SPPs over a broad spectral range.[10,15−19] The antenna radiation from the electron-beam excited resonant modes can be readily detected and spectrally resolved with the use of a scanning electron microscope coupled to an external spectrometer. This electron-induced optical emission is termed cathodoluminescence (CL). We resolve with deep-subwavelength resolution the plasmon standing waves and find the odd-order SR-SPP resonances observed earlier in optical scattering, as well as even-order resonances that are hidden in

Received: July 3, 2011
Revised: August 28, 2011
Published: August 31, 2011

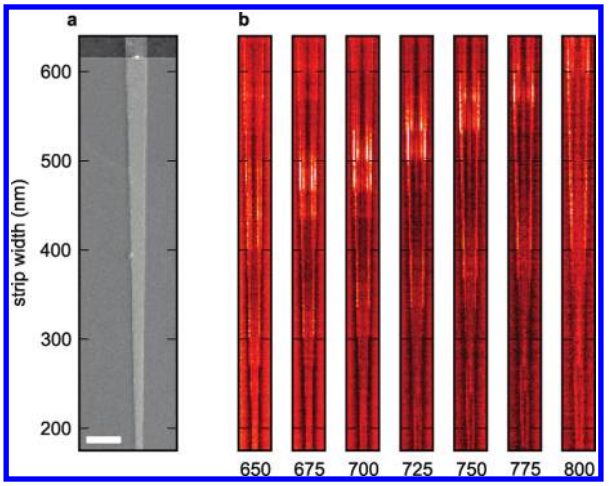

Figure 1. (a) Scanning electron microscopy image of a 20 nm thick Ag wedge on a silicon-on-insulator (SOI) substrate. The *y*-axis denotes the strip width at different locations along the length of the wedge. The scale bar is 1 μm. (b) Spatially resolved cathodoluminescence scans of the Ag wedge taken with 30 keV electrons and collected at different emission wavelengths in the range from 650 to 800 nm. Width- and wavelength-dependent resonant bands with higher CL signal are clearly resolved in the images.

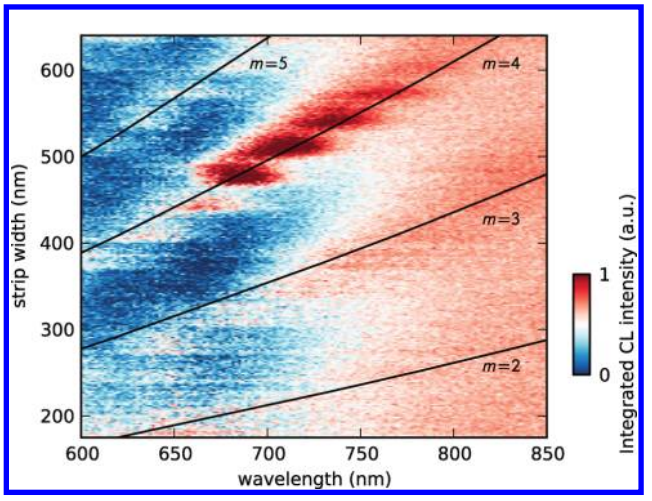

Figure 2. Cathodoluminescence (CL) signal integrated along the strip width, plotted as a function of strip width and emission wavelength. Four resonant bands exhibiting enhanced CL are clearly resolved. The drawn lines are calculated using eq 1 and indicate the Fabry–Pérot resonances of short-range surface plasmon polaritons (SR-SPPs) for different mode orders $m = 2-5$.

top-illumination experiments. We also find that in addition to the short-range SPPs[5,6] the long-range SPPs play a critical role in the operation of strip antennas.

Figure 1a shows a tapered Ag wedge that is the focus of the current study. This wedge can locally be viewed as a nanostrip antenna of a specific width (indicated on the vertical axis), allowing for study of many antenna sizes within one fabricated structure. The 20 nm thick Ag wedge antenna was fabricated on a silicon-on-insulator substrate (20 nm SiO_2 spacer on top of 40 nm of Si on a 400 nm buried oxide attached to a Si wafer), using electron-beam lithography, Ag evaporation, and lift-off, as described in previous work.[6] Spectrally resolved CL scans of the antenna were made using a 30 kV electron beam focused to a diameter of 10 nm at a typical beam current of 1 nA. A two-dimensional map of CL spectra with a pixel pitch of 10 nm was measured by collecting radiation as a function of beam position on the sample and then analyzing the radiation with a spectrometer. This CL radiation is collected by a parabolic mirror (1.46π sr. acceptance angle) placed between the sample and the pole-piece of the microscope. Measured CL spectra have contributions from both antenna resonances and background radiation from the substrate. The CL spectra shown have this background radiation removed.

Figure 1b shows the CL signal as function of electron-beam position on the wedge for seven equally spaced emission wavelengths in the range from 650 to 800 nm. Each image in Figure 1b shows regions/widths along the wedge where the CL signal is clearly enhanced. We will argue that these signal enhancements can be attributed to the excitation of standing wave SPP resonances. Similar bright bands have been observed and attributed to standing wave SPP resonances in nanowire antennas[16,20] and plasmonic Fabry–Pérot cavities fashioned into a single-crystal Au surface.[21] This interpretation is also consistent with the fact that the brighter regions move up along the wedge (to larger widths) as the wavelength of the collected emission is increased. The linear movement of these bright regions with emission wavelength reflects the approximately linear dependence of the SPP resonant wavelengths on strip width.

To explore the dependence of the resonant wavelengths on the strip width, we plot in Figure 2 the integrated CL intensity across the width of the strip for different strip widths and wavelengths. This figure shows four resonant bands. We model the resonances using a Fabry–Pérot model,[2,3] in which a resonance condition is met if the antenna width w equals an integer multiple of half SPP wavelengths including a phase advance ϕ upon reflection from the sides of the wedge

$$w_{\mathrm{res},m} = \left[m - \frac{\phi}{\pi}\right]\frac{\lambda_o}{2n_{\mathrm{spp}}} \qquad (1)$$

Here m indicates the order of the resonance, λ_o is the free-space wavelength and n_{spp} the mode index. In the following, we first presuppose that the antenna behavior is dominated by the antisymmetric short-range SPP mode, with a mode index $n_{\mathrm{sr-spp}}$. The drawn lines in Figure 2 labeled by the resonance order $m = 2-5$ are calculated using eq 1 using $\phi = \pi/2$ and a frequency-dependent $n_{\mathrm{sr-spp}}$ ranging between 2.2 and 2.7. These values were previously determined using numerical simulations[3,22] and experiments.[5,6] The solid lines in Figure 2 are calculated using eq 1 and correspond well to the measured data. Unlike in normal incidence receiving mode where only odd SR-SPP resonances are observed,[6] this CL resonance map reveals both even ($m = 2,4$) and odd ($m = 3,5$) resonances. The electron beam effectively serves as a broadband localized dipole source as it passes through the metal surface. This transition dipole is composed of the incident moving electron charge and its image charge with the metal. As a radiating dipole source it can emit into the allowed optical modes (including both even and odd antenna modes) at the location of scanning electron beam. The emission from the antenna modes could subsequently be collected with a parabolic mirror that can collect photons over a broad angular range.

Next, we focus on the fine structure in the CL signal across the width of the antenna. Figure 3a shows a CL emission map taken at an emission wavelength of 700 nm. The image shows fringes that become more pronounced near the resonant widths marked

dx.doi.org/10.1021/nl202256k |*Nano Lett.* 2011, 11, 4265–4269

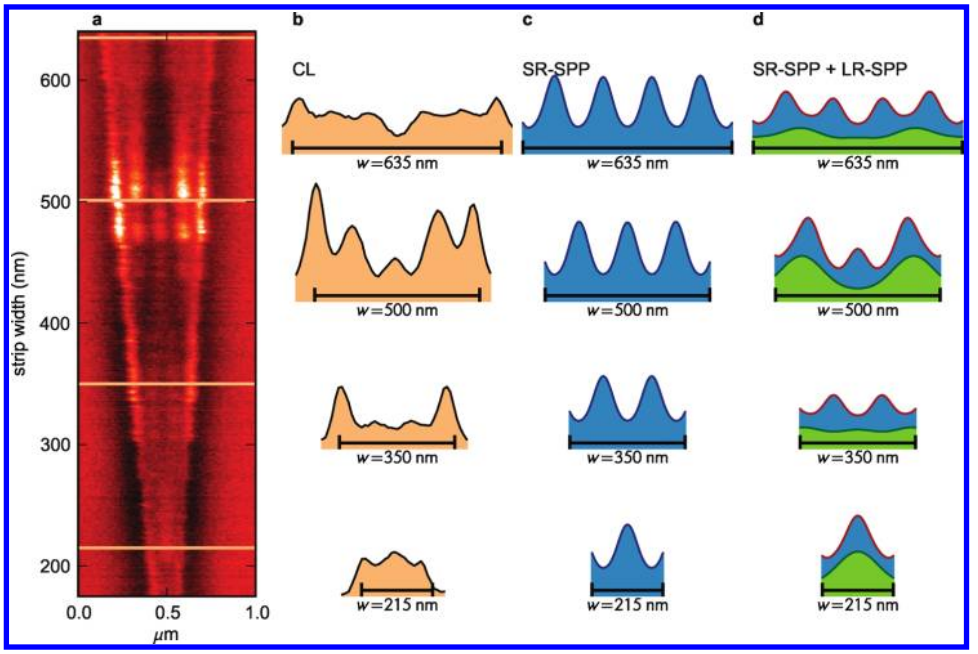

Figure 3. (a) Cathodoluminescence image for a free-space emission wavelength of 700 nm. The scan has been stretched 4 times in the horizontal direction to more clearly show the fine structure across the width of the antenna. Horizontal lines denote widths at which resonances occur. (b) Line cuts of the CL signal taken at resonant widths from the image in (a), showing SPP standing wave patterns. (c) Calculated intensity of SPP standing waves according to the Fabry–Pérot model for short-range SPP resonant modes. (d) Calculated intensity of SPP standing Fabry–Pérot model for a superposition of resonant short-range and long-range SPP modes.

by horizontal yellow lines (derived from eq 1 and Figure 2). The CL intensity along these lines is shown in Figure 3b. The fringes in these line cuts are dominated by the standing SPP wave pattern of the resonant strip, with peaks spaced by approximately $\lambda_{sr\text{-}spp}/2$. The standing wave patterns each have a number of nodes and antinodes commensurate with their resonance order (number of antinodes within the cavity equals $m - 1$). The intensity of the plasmonic standing wave pattern at a position x along the strip width derived from the Fabry–Pérot model is given by

$$I(x) \propto \left| \frac{re^{ikx} - e^{-ikx}}{1 - r^2 e^{i2kw}} \left(e^{ikx} - re^{-ikx} e^{i2kw}\right) \right|^2 \qquad (2)$$

Here $k = n_{spp}k_o$ is the propagation constant of the relevant SPP, and r is the complex SPP reflection coefficient that takes into account the phase advance upon reflection.[3] Figure 3c shows calculations of eq 2 for the resonant widths in Figure 3b for short-range asymmetric SPPs. Comparing Figure 3 panels b and c it is clear that the model correctly predicts both the number and position of the minima and maxima in the CL scans. It does not account for the bright peaks at the ends of the strip. However, similar peaks commonly occur near truncations of a metallic structure[16,21] and can be ascribed to a locally enhanced coupling of the electron beam to SPPs. In addition to this expected discrepancy between Figure 3 panels b and c, we note two other features in the CL data in Figure 3a,b that cannot be explained by the single-mode SR-SPP resonance model shown in Figure 3c. First, in the experiment the peak heights of the standing wave are nonuniform across the width while in the Fabry–Pérot model all of the peaks have the same height. Second, the model shows a monotonically decreasing visibility of the standing wave pattern for increasing width, due to increased SPP propagation losses,

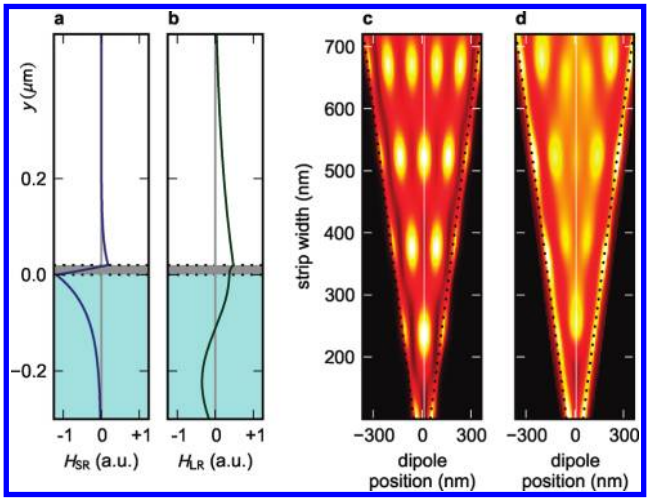

Figure 4. (a,b) Calculated mode profiles (transverse magnetic field amplitude) for (a) short-range and (b) long-range SPP modes for a 20 nm thick Ag film on an n = 1.87 substrate. (c,d) Calculated distribution of the local density of optical states (LDOS) for a point dipole placed in the substrate below the strip (c) and above the strip (d).

while in experiment the m = 4 (w = 500 nm) resonance is more intense than the m = 2 and 3 resonance.

To explain these two observations we must invoke the symmetric long-range SPP mode as an additional relevant resonant antenna mode. For symmetry reasons, this mode is also hidden in optical experiments where the antenna is illuminated from the top and to our knowledge this mode has in fact remained elusive in optical scattering experiments. Figure 4a shows the calculated transverse magnetic field mode amplitude profiles for a free-space wavelength of λ_o = 700 nm for the short-range antisymmetric

dx.doi.org/10.1021/nl202256k |*Nano Lett.* 2011, 11, 4265–4269

(a) and the long-range symmetric (b) SPP mode.[22] In the calculations, the layered SOI substrate was modeled by a bulk substrate with an effective $n_{sub} = 1.87$ and optical constants for Ag were taken from Rakić.[23] We note that the LR-SPP is a leaky mode in this case due to the high index of the substrate. In the CL experiment, the electron beam couples to both of these SPP modes. In Figure 3d, we plot the intensity of the sum of short-range and long-range SPP Fabry−Pérot standing waves calculated using eq 2 . We assume their relative contributions are equal and a reflection phase of the LR-SPP of $3\pi/2$. The individual contributions from long-range and short-range SPPs are plotted in green and blue, respectively. The summed intensity shows good quantitative agreement with the experimental line plots in Figure 3b. The simulations accurately predict the deep minimum at the center of the strip for the largest width (w = 635 nm). The reduced intensity at the center of the CL scan for the w = 500 nm width region is also reproduced. Finally, the simulations also show the enhanced intensity in the center of the narrowest strip ($m_{SR} = 2$). The strong modulation of the intensity maxima across the antenna width are the result of the large difference in wavelength of the short-range and long-range modes, as is also evident from Figure 3d. For an antenna width w = 500 nm both SPP modes are resonant ($m_{LR} = 2$ resonance for the long-range SPP; $m_{SR} = 4$ resonance for the short-range SPP), leading to a strongly enhanced integrated intensity, as is also observed experimentally in Figure 3b. In contrast, for w = 350 nm the short-range SPP is resonant while the long-range SPP is not, leading to the relatively weak intensity profile for the latter.

To further study the contribution of the two SPP modes to the antenna radiation, we performed simulations of the local density of optical states (LDOS) near the top and bottom surface of the antenna. We use two-dimensional finite-difference frequency-domain (FDFD)[24] electromagnetic simulations to model a vertically oriented dipole placed 15 nm from the metal surface and use a substrate with an effective index of $n_{sub} = 1.87$. Figure 4c shows the two-dimensional LDOS distribution for dipoles placed in the substrate below the antenna. The intensity distribution matches quite well with the calculated line scans for the short-range SPP mode in Figure 3c. This indicates that emitters placed below the antenna predominantly couple to short-range SPPs. Interestingly, the LDOS above the antenna (Figure 4d) shows a very different distribution. We attribute this to the superimposed standing wave patterns of both short-range and long-ranges SPPs. Indeed, the calculated integrated intensity distributions in Figure 3d are in good agreement with the corresponding cuts through Figure 4d. This also helps to validate our assumption of equal relative contributions from LR and SR SPP resonances.

The difference in the two-dimensional LDOS profiles for the two dipole positions is explained by the difference in coupling to the SPP mode profiles. A dipole placed in the substrate below the antenna will couple most strongly to the short-range SPP due to large mode overlap between the dipole field and the short-range SPP mode profile (see in Figure 4a). For a dipole placed above the antenna, we find a comparable mode overlap with both types of SPP modes and both modes are thus excited. As the electron beam is a direct probe of the LDOS along its trajectory, and since it passes through both the top and bottom interfaces, the CL measurement includes contributions from both top and bottom LDOS patterns. This is consistent with the observation of both short-range and long-range SPP resonances in the CL scans.

In conclusion, we have investigated the resonant modes of plasmonic strip antennas using high-resolution cathodoluminescence imaging spectroscopy. From the observed CL distributions, we directly characterize the relevant resonant modes supported by the antenna. We find that both short-range and long-range SPP modes play a critical role in the resonant optical behavior of the antenna. The superposition of these modes gives rise to a complex CL intensity profile across the antenna. The importance of the contributions of short-range and long-range SPPs to the CL signal is further confirmed using calculations of the local density of states. We find that a dipole placed in the substrate below the antenna preferentially couples to the short-range SPP, while a dipole placed above the antenna excites both types of SPP modes. This work resolves the full modal distribution of a plasmonic strip antenna, including modes previously hidden in optical experiments. It demonstrates some similarities and fundamental differences between resonant antenna modes excited by far field plane-wave radiation and those excited in the near-field. The obtained results can help guide the design of plasmonic structures as transmitting optical antennas.

AUTHOR INFORMATION

Corresponding Author
*E-mail: brongersma@stanford.edu.

ACKNOWLEDGMENT

The authors would like to thank Ragip A. Pala for assistance in preparation of the samples used in this work. The Stanford part of this work is supported by the Center for Advanced Molecular Photovoltaics (Award No KUS-C1-015-21), made by King Abdullah University of Science and Technology (KAUST). CL experiments were performed at AMOLF and are part of the research program of FOM that is financially supported by NWO. Work at AMOLF is also supported by NanoNextNL, a nanotechnology program of the Dutch Ministry of Economic Affairs. It is also part of the research program "Microscopy and modification of nanostructures with focused electron and ion beams" that is cofinanced by FEI Company.

REFERENCES

(1) Novotny, L.; van Hulst, N. *Nat. Photonics* **2011**, *5*, 83–90.
(2) Søndergaard, T.; Bozhevolnyi, S. I. *Opt. Express* **2007**, *15*, 4198–4204.
(3) Barnard, E. S.; White, J. S.; Chandran, A.; Brongersma, M. L. *Opt. Express* **2008**, *16*, 16529–16537.
(4) Farhang, A.; Martin, O. J. F. *Opt. Express* **2011**, *19*, 11387–11396.
(5) Søndergaard, T.; Beermann, J.; Boltasseva, A.; Bozhevolnyi, S. I. *Phys. Rev. B* **2008**, *77*, 115420.
(6) Barnard, E. S.; Pala, R. A.; Brongersma, M. L. *Nat. Nanotechnol.* **2011**, *9*, 588–593.
(7) Liu, N.; Langguth, L.; Weiss, T.; Kastel, J.; Fleischhauer, M.; Pfau, T.; Giessen, H. *Nat. Mater.* **2009**, *8*, 758–762.
(8) Luk'yanchuk, B.; Zheludev, N. I.; Maier, S. A.; Halas, N. J.; Nordlander, P.; Giessen, H.; Chong, C. T. *Nat. Mater.* **2010**, *9*, 707–715.
(9) Koh, A. L.; Bao, K.; Khan, I.; Smith, W. E.; Kothleitner, G.; Nordlander, P.; Maier, S. A.; McComb, D. W. *ACS Nano* **2009**, *3*, 3015–3022.
(10) García de Abajo, F. J. *Rev. Mod. Phys.* **2010**, *82*, 209–275.
(11) Economou, E. N. *Phys. Rev.* **1969**, *182*, 539–554.
(12) Berini, P. *Phys. Rev. B* **2000**, *61*, 10484–10503.
(13) Dionne, J. A.; Sweatlock, L. A.; Atwater, H. A.; Polman, A. *Phys. Rev. B* **2005**, *72*, 075405.

(14) Verhagen, E.; Spasenović, M.; Polman, A.; Kuipers, L. K. *Phys. Rev. Lett.* **2009**, *102*, 203904.
(15) van Wijngaarden, J. T.; Verhagen, E.; Polman, A.; Ross, C. E.; Lezec, H. J.; Atwater, H. A. *Appl. Phys. Lett.* **2006**, *88*, 221111.
(16) Vesseur, E. J. R.; de Waele, R.; Kuttge, M.; Polman, A. *Nano Lett.* **2007**, *7*, 2843–2846.
(17) Kuttge, M.; Vesseur, E. J. R.; Koenderink, A. F.; Lezec, H. J.; Atwater, H. A.; Garca de Abajo, F. J.; Polman, A. *Phys. Rev. B* **2009**, *79*, 113405.
(18) Vesseur, E. J. R.; García de Abajo, F. J.; Polman, A. *Nano Lett.* **2009**, *9*, 3147–3150.
(19) Coenen, T.; Vesseur, E. J. R.; Polman, A.; Koenderink, A. F. *Nano Lett.* **2011**, in press, doi 10.1021/nl201839g.
(20) Nicoletti, O.; Wubs, M.; Mortensen, N. A.; Sigle, W.; van Aken, P. A.; Midgley, P. A. *Opt. Express* **2011**, *19*, 15371–15379.
(21) Kuttge, M.; Vesseur, E. J. R.; Polman, A. *Appl. Phys. Lett.* **2009**, *94*, 183104.
(22) Kekatpure, R. D.; Hryciw, A. C.; Barnard, E. S.; Brongersma, M. L. *Opt. Express* **2009**, *17*, 24112–24129.
(23) Rakić, A. D.; Djurišić, A. B.; Elazar, J. M.; Majewski, M. L. *Appl. Opt.* **1998**, *37*, 5271.
(24) Veronis, G.; Fan, S. In *Surface Plasmon Nanophotonics*; Brongersma, M. L., Kik, P. G., Eds.; Springer, New York, 2007; Vol. 131, pp 169−182.